

# Emergent quantum criticality from spin-orbital entanglement in $d^8$ Mott insulators: the case of a diamond lattice antiferromagnet

Fei-Ye Li<sup>1</sup> and Gang Chen<sup>1,2,3\*</sup>

<sup>1</sup>State Key Laboratory of Surface Physics and Department of Physics, Fudan University, Shanghai 200433, China

<sup>2</sup>Center for Field Theory and Particle Physics, Fudan University, Shanghai 200433, China and

<sup>3</sup>Collaborative Innovation Center of Advanced Microstructures, Nanjing University, Nanjing 210093, China

(Dated: August 21, 2018)

Motivated by the recent activities on the Ni-based diamond lattice antiferromagnet  $\text{NiRh}_2\text{O}_4$ , we theoretically explore on a general ground the unique spin and orbital physics for the  $\text{Ni}^{2+}$  ions with a  $3d^8$  electron configuration in the tetrahedral crystal field environment and on a diamond lattice Mott insulator. The superexchange interaction between the local moments usually favors magnetic orders. Due to the particular electron configuration of the  $\text{Ni}^{2+}$  ion with a partially filled upper  $t_{2g}$  level and a fully filled lower  $e_g$  level, the atomic spin-orbit coupling becomes active at the linear order and would favor a spin-orbital-entangled singlet with quenched local moments in the single-ion limit. Thus, the spin-orbital entanglement competes with the superexchange and could drive the system to a quantum critical point that separates the spin-orbital singlet and the magnetic order. We further explore the effects of magnetic field and uniaxial pressure. The non-trivial response to the magnetic field is *intimately* tied to the underlying spin-orbital structure of the local moments. We discuss the future experiments such as doping and pressure, and point out the correspondence between different electron configurations.

*Introduction.*—The spin-orbit coupling (SOC) is a relativistic effect and plays an important role in our understanding of the quantum mechanical properties of quantum materials with heavy elements. Contrary to this conventional belief that explains the recent SOC activities in  $4d/5d$  transition metal compounds [1], SOC occasionally becomes important in  $3d$  transition metal materials, especially in the Mott insulating systems with orbital degeneracies [2]. It is well-known that, in Mott insulators with pure spin moments, the atomic SOC enters via the high order perturbation of the Hubbard model and generates the single-ion spin anisotropy and the Dzyaloshinskii-Moriya interaction [2]. Except under certain circumstances, these extra spin anisotropy and interactions can often be regarded as small perturbations to the (Heisenberg) exchange part of the interactions. When the system has an orbital degeneracy, however, the atomic SOC should be considered at the first place and would reconstruct local spin and orbital degrees of freedom. The diamond lattice antiferromagnet  $\text{FeSc}_2\text{S}_4$  [3–12] and various vanadates [2, 13–15] provide physical realizations of such physics, where the former has an  $e_g$  orbital degeneracy while the latter has a  $t_{2g}$  degeneracy.

In this Letter, we study a diamond lattice antiferromagnet where the  $\text{Ni}^{2+}$  ions are the magnetic ions. We are partly motivated by the experiments and the existence of the diamond lattice antiferromagnet  $\text{NiRh}_2\text{O}_4$  [16], and explore on a general ground the consequence of the atomic SOC of the  $\text{Ni}^{2+}$  ions. We point out that there exists a keen competition between the atomic SOC at the single-ion level and the inter-site superexchange interaction for the  $3d$  transition metal ion like  $\text{Ni}^{2+}$ . The spin-orbital singlet would give way to the magnetically ordered state through a quantum phase transition when the superexchange interaction dominates over

the atomic SOC. We further show the effect of the external magnetic field and the uniaxial pressure on the quantum criticality. The non-trivial structure of the phase diagram such as the re-entrant transition under the field directly reveals the underlying spin-orbital structure of the local moments. Although our motivation originates partly from the diamond lattice antiferromagnet  $\text{NiRh}_2\text{O}_4$ , the physics that we reveal in this Letter may be well extended to other magnets with similar crystal field schemes and orbital configurations. We further go beyond the specific case of the  $\text{Ni}^{2+}$  ions, establish the *correspondence* between different electron configurations, and suggest the applicability to many other materials.

*The microscopics and the model.*—We start with the microscopics of the  $\text{Ni}^{2+}$  ion. In  $\text{NiRh}_2\text{O}_4$ , the  $\text{Ni}^{2+}$  ion is in the tetrahedral crystal field environment, and as a result, the  $t_{2g}$  levels are higher in energy than the  $e_g$  levels. As we show in Fig. 1, the lower  $e_g$  levels are completely filled, and the  $t_{2g}$  levels are partially filled with four elec-

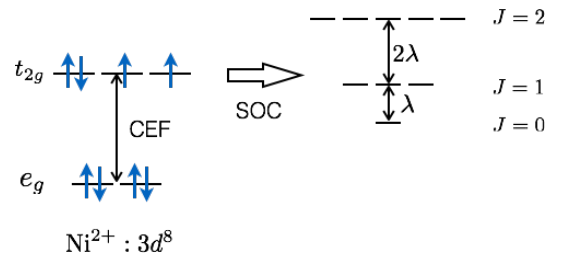


FIG. 1. (Color online.) The electron configuration of the  $\text{Ni}^{2+}$  ion in the tetrahedral crystal field environment. When the atomic spin-orbit coupling (SOC) is introduced, the electron states in the upper  $t_{2g}$  levels are further split into the spin-orbital entangled  $J$  states. In the figure, “CEF” refers to the crystal electric field splitting.

trons. For our purpose here, we first ignore the further splitting within the  $t_{2g}$  manifold and include this specific physics for  $\text{NiRh}_2\text{O}_4$  in the later part of the Letter. Because the  $t_{2g}$  levels are partially filled, the atomic SOC is active at the linear order. As the fully-filled  $e_g$  manifold can be neglected, the local physics for the  $3d^8$  electron configuration here is rather analogous to the one for the  $4d^4/5d^4$  electron configurations of the  $\text{Ru}^{4+}$  or  $\text{Ir}^{5+}$  ions that have been discussed in Refs. 17 and 18, where the latter [18] proposed the possibility of excitonic magnetism. For the  $t_{2g}$  manifold in Fig. 1, the local Hund's coupling first favors a total spin  $S = 1$  local moment, and the remaining orbital occupation still has a three-fold degeneracy. The total orbital angular momentum remains unquenched and can be treated as an *effective* orbital angular moment  $\mathbf{L}$  with  $L = 1$  in the reduced Hilbert space of the three orbital occupations. The atomic SOC is then written as

$$H_{\text{soc}} = +\lambda \sum_i \mathbf{L}_i \cdot \mathbf{S}_i, \quad (1)$$

where the sign of the SOC is opposite to the case for two electrons in the  $t_{2g}$  manifold. The SOC here acts on the total spin and total orbital angular momentum of the four electrons and differs from the SOC at the single electron level. The SOC entangles the spin and the orbitals and leads to a total moment  $J$  in the single ion limit. The single-ion ground state is a spin-orbital singlet with  $J = 0$ , and the excited ones are  $J = 1$  triplets and  $J = 2$  quintuplets (see Fig. 1).

Besides the atomic SOC, the spin and orbital degrees of freedom on neighboring sites interact with each other through the superexchange interaction. Due to the orbital degeneracy, the exchange interaction should be of the Kugel-Khomskii form [19]. The superexchange path for both first neighbor and second neighbor in  $\text{NiRh}_2\text{O}_4$  is given by Ni-O-Rh-O-Ni and involves five atoms. Thus, the explicit derivation of the superexchange interaction is complicated and is not quantitatively reliable. Our purpose here is not to be quantitatively precise, but is to capture the generic physics of the competition between the spin-orbital entanglement and the tendency to magnetic ordering for the Ni-based magnets and the systems alike. Thus, we consider a simplified superexchange model with only spin interactions. The exchange model is given as

$$\begin{aligned} H_{\text{ex}} &= \sum_{ij} J_{ij} \mathbf{S}_i \cdot \mathbf{S}_j \\ &= \sum_{\langle ij \rangle} J_1 \mathbf{S}_i \cdot \mathbf{S}_j + \sum_{\langle\langle ij \rangle\rangle} J_2 \mathbf{S}_i \cdot \mathbf{S}_j, \end{aligned} \quad (2)$$

where  $J_1$  ( $J_2$ ) is the first (second) neighbor exchange coupling. This simplified model captures the ordering tendency, but is not supposed to capture the possibility of an (exotic) quantum spin-orbital liquid with fractionalized excitations [20].

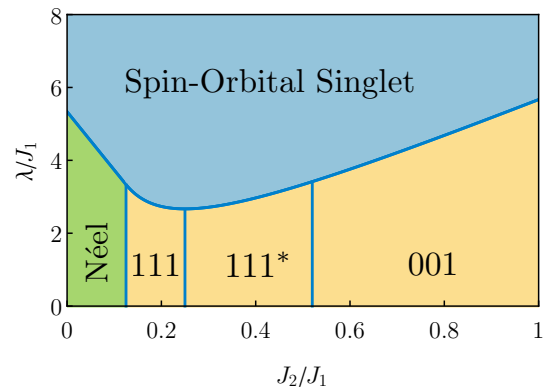


FIG. 2. (Color online.) The phase diagram of the full model in Eq. (3). This phase diagram summarizes the competition between the SOC and the superexchange interaction and captures the frustration of the exchange part. Please refer to the main text for details about the magnetic orders.

*Phase diagram and quantum criticality.*—Here we study the full Hamiltonian that contains both SOC and exchange interaction with,

$$H = H_{\text{soc}} + H_{\text{ex}}. \quad (3)$$

Once our full model is written, the physics is almost transparent. Besides the competition between SOC and exchange, the exchange frustration would further complicate our phase diagram. To establish the phase diagram, one approach is to start from the (non-magnetic) spin-orbital singlet phase and study its magnetic instability to an ordered state by condensing the excitonic excitation. The resulting ordered state was dubbed “excitonic magnetic state”. This approach was used by G. Khaliullin for a more realistic exchange model on a square lattice [18] with  $4d^4/5d^4$  ions such as  $\text{CaRu}_2\text{O}_4$  by truncating the physical Hilbert space to the  $J = 0$  and  $J = 1$  states. The other approach is to start from the ordered state and tracing the fate of the magnetic order parameters as we increase the strength of the SOC. When the magnetic order disappears, the system enters the spin-orbital singlet phase. Both approaches are adopted in this work. Via a Weiss-type mean-field decoupling, our Hamiltonian becomes

$$\begin{aligned} H \rightarrow H_{\text{MFT}} &= H_{\text{soc}} + \sum_{\langle ij \rangle} J_1 \mathbf{S}_i \cdot \langle \mathbf{S}_j \rangle \\ &\quad + \sum_{\langle\langle ij \rangle\rangle} J_2 \mathbf{S}_i \cdot \langle \mathbf{S}_j \rangle, \end{aligned} \quad (4)$$

where  $\langle \mathbf{S}_j \rangle$  is taken as a mean-field order parameter. To choose a mean-field ansatz for the order parameter, we start from the limiting case with a vanishing SOC such that this limit has been well-understood. Here we consider the antiferromagnetic couplings  $J_1 > 0$  and  $J_2 > 0$ . It was shown that [20–22], for  $J_2/J_1 < 1/8$ , a Néel state with an order wavevector  $\mathbf{q} = \mathbf{0}$  is obtained; for

$J_2/J_1 > 1/8$ , the ground state has a spiral configuration, and the degenerate order wavevectors form a spiral surface [20] in momentum space and satisfy

$$\cos \frac{q_x}{2} \cos \frac{q_y}{2} + \cos \frac{q_x}{2} \cos \frac{q_z}{2} + \cos \frac{q_y}{2} \cos \frac{q_z}{2} = \frac{J_1^2}{16J_2^2} - 1. \quad (5)$$

When  $J_2/J_1$  is increased from  $1/8$ , this “spiral surface” emerges and surrounds  $\mathbf{q} = \mathbf{0}$ , showing a nearly spherical geometry. It then touches the boundary of the Brillouin zone at  $J_2/J_1 = 1/4$  and develops “holes” on the boundary of the Brillouin zone, as  $J_2/J_1$  is further increased. Finally, the spiral surface shrinks to lines corresponding to the degenerate ground state manifold of two decoupled face centered cubic lattices in the limit  $J_2/J_1 \rightarrow \infty$ . This degeneracy is lifted when quantum fluctuation is included, giving certain stabilized spiral orders [23–25]. For  $1/8 < J_2/J_1 < 1/4$ , the selected wavevectors are along the [111] direction. For  $1/4 < J_2/J_1 \lesssim 1/2$ , the [111] direction no longer intersects with the spiral surface and the selected wavevectors are around the [111] direction. This region is labeled by [111\*] in Fig. 2. When  $J_2/J_1 \gtrsim 1/2$ , quantum fluctuation favors the spiral orders with the wavevectors along the [001] direction.

From the known results, we set up a general mean-field ansatz as

$$\begin{aligned} \mathbf{r}_j \in \text{I}, \quad \langle \mathbf{S}_j \rangle &= \mathbb{M} \text{Re}[(\hat{x} - i\hat{y})e^{i\mathbf{q}\cdot\mathbf{r}_j}], \\ \mathbf{r}_j \in \text{II}, \quad \langle \mathbf{S}_j \rangle &= \mathbb{M} \text{Re}[(\hat{x} - i\hat{y})e^{i(\mathbf{q}\cdot\mathbf{r}_j + \phi_q)}], \end{aligned} \quad (6)$$

where “I” and “II” refer to the two sublattices of the diamond lattice,  $\mathbf{q}$  is the propagating wave vector of the spin spiral and  $\phi_q$  is the phase shift between the two sublattices [20]. The order parameter  $\mathbb{M}$  is determined self-consistently from the mean-field Hamiltonian  $H_{\text{MFT}}$ .

Our phase diagram is depicted in Fig. 2. When SOC is weak, the magnetic ordered phase is separated into the Néel order region and the spiral order regions (111, 111\* and 001). A transition from magnetic ordered phase to the spin-orbital singlet (SOS) occurs when increasing the strength of SOC. This transition is evidenced by the vanishing of  $\mathbb{M}$  and is found to be continuous within our mean-field theory. The critical strength of SOC is  $16(J_1/3 - J_2)$  for  $J_2/J_1 < 1/8$  and  $J_1^2/(3J_2) + 16J_2/3$  for  $J_2/J_1 > 1/8$ . As expected, when the frustration is large, a smaller critical SOC is needed to drive the transition. The smallest critical SOC is found at  $J_2/J_1 = 1/4$ .

To explore the critical properties, we start from the spin-orbital singlet and study its excitations and instability [18, 26]. Removing the highly excited  $J = 2$  quintuplets, we then rewrite our model using a representation with four flavors of bosons  $s_i, t_{ix}, t_{iy}, t_{iz}$  on each site  $i$

that are defined as

$$s_i^\dagger |0\rangle \equiv |0, 0\rangle_i, \quad (8)$$

$$t_{ix}^\dagger |0\rangle \equiv i(|1, 1\rangle_i - |1, -1\rangle_i)/\sqrt{2}, \quad (9)$$

$$t_{iy}^\dagger |0\rangle \equiv (|1, 1\rangle_i + |1, -1\rangle_i)/\sqrt{2}, \quad (10)$$

$$t_{iz}^\dagger |0\rangle \equiv -i|1, 0\rangle_i, \quad (11)$$

where the states are labeled  $|J, J^z\rangle$  and  $|0\rangle$  is the vacuum state. A local Hilbert space constraint  $s_i^\dagger s_i + \sum_\alpha t_{i\alpha}^\dagger t_{i\alpha} = 1$  is imposed with  $\alpha = x, y, z$ . In the spin-orbital singlet phase, the singlet boson  $s_i$  is condensed with  $\langle s_i \rangle \equiv s \neq 0$ . With the above reformulation of the spin variables, we obtain a flavor-wave mean-field Hamiltonian for the triplet excitations,

$$H_{\text{MF}} = \sum_{ij,\alpha} \frac{2J_{ij}}{3} (t_{i\alpha}^\dagger t_{j\alpha} + t_{i\alpha}^\dagger t_{j\alpha}^\dagger) + \lambda \sum_{i\alpha} t_{i\alpha}^\dagger t_{i\alpha}, \quad (12)$$

where the detailed derivation is given in the Supplementary Material [27], and the triplon excitation is found as

$$\omega^\pm(\mathbf{q}) = \lambda^{\frac{1}{2}} (\lambda + 4J_{\mathbf{q}}^\pm/3)^{\frac{1}{2}}, \quad (13)$$

with  $J_{\mathbf{q}}^\pm \equiv J_2 \sum_{\mathbf{b}_i} e^{i\mathbf{q}\cdot\mathbf{b}_i} \pm J_1 |\sum_{\mathbf{a}_i} e^{i\mathbf{q}\cdot\mathbf{a}_i}|$ , and  $\{\mathbf{a}_i\}$  ( $\{\mathbf{b}_i\}$ ) refer to the first (second) neighbor vectors. Both  $\omega^\pm(\mathbf{q})$  are three-fold degenerate and the minimum of  $\omega^-(\mathbf{q})$  is determined by minimizing  $J_{\mathbf{q}}^-$ . For  $J_2/J_1 < 1/8$ , a single minimum is realized at the  $\Gamma$  point, and for  $J_2/J_1 > 1/8$ , the minima are extensively degenerate and realized on the “spiral surface”.

The triplon gap is closed at a critical SOC that coincides with the Weiss mean-field result. For  $J_2/J_1 > 1/8$ , the enhanced density of states at low energies at the criticality implies a specific heat behavior  $C_v \propto T$  at low temperatures [23, 28]. This behavior should be modified at the zero-temperature limit since the accidental continuous degeneracy in momentum space would be lifted by fluctuations. On the other hand, for  $J_2/J_1 < 1/8$ , there is only a single critical mode at the criticality, hence one expects a conventional  $C_v \propto T^3$  behavior up to a logarithmic correction from fluctuations beyond the mean-field theory.

*Response to magnetic field.*—The response to external magnetic field provides an important and visible characterization of the phase transition from the spin-orbital singlet to the ordered phase. It is of experimental interest to understand whether the magnetic field enhances the magnetic order like the case for the dimerized magnets [29] or suppresses the magnetic order like the case for  $\text{FeSc}_2\text{S}_4$  [3, 4, 6, 7]. We consider the Zeeman coupling,  $H_{\text{Zeeman}} = -\sum_i B(L_i^z + 2S_i^z)$ , and the mean-field Hamiltonian becomes  $H_{\text{MFT}}' = H_{\text{MFT}} + H_{\text{Zeeman}}$ .

With the magnetic field, the mean-field ansatz is

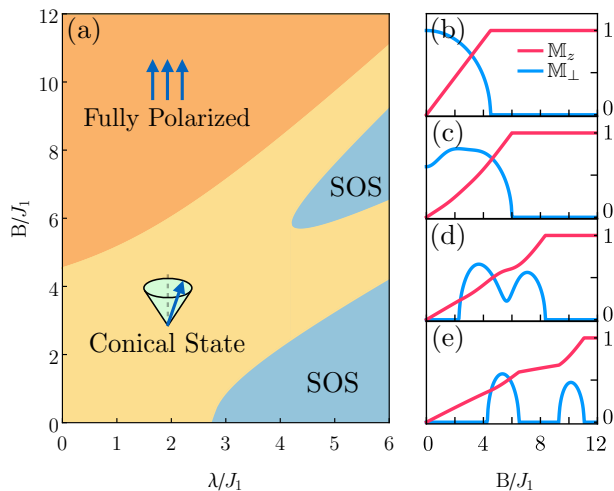


FIG. 3. (Color online.) The left panel is the phase diagram under external magnetic fields. We have fixed  $J_2/J_1 = 1/4$  in the plot. Here, ‘‘SOS’’ refers to spin-orbital singlet. There is a region that supports re-entrant transitions between the conical state and the SOS state as the field is varied. The right panel depicts the magnetization curves for  $\lambda/J_1 = 0, 2, 4, 6$  from top to bottom.

adapted as

$$\mathbf{r}_j \in \text{I}, \quad \langle \mathbf{S}_j \rangle = \mathbb{M}_\perp \text{Re}[(\hat{x} - i\hat{y})e^{i\mathbf{q}\cdot\mathbf{r}_j}] + \mathbb{M}_z \hat{z}, \quad (14)$$

$$\mathbf{r}_j \in \text{II}, \quad \langle \mathbf{S}_j \rangle = \mathbb{M}_\perp \text{Re}[(\hat{x} - i\hat{y})e^{i(\mathbf{q}\cdot\mathbf{r}_j + \phi_q)}] + \mathbb{M}_z \hat{z}, \quad (15)$$

where  $\mathbb{M}_\perp$  and  $\mathbb{M}_z$  are determined self-consistently from the mean-field Hamiltonian  $H'_{\text{MFT}}$  and represent the magnetizations on the  $xy$  plane and along the  $z$  axis, respectively.

In Fig. 3, we depict the phase diagram of  $H'_{\text{MFT}}$  for a fixed  $J_2/J_1$ . The response to external magnetic field varies for different strength of the SOC, and more precisely, differs significantly for the initial state of the system at the zero field, and thus provides a characterization of the ground state. In the limit  $\lambda \rightarrow 0$ ,  $H'_{\text{MFT}}$  reduces to  $H_{\text{ex}} + H_{\text{Zeeman}}$ . From the initial spiral order, our mean-field theory yields  $\mathbb{M}_\perp = [1 - (B/\tilde{J})^2]^{1/2}$  and  $\mathbb{M}_z = B/\tilde{J}$  when  $B < \tilde{J}$ , where

$$\tilde{J} \equiv \begin{cases} 4J_1, & \text{for } J_2/J_1 < 1/8, \\ J_1^2/(8J_2) + 8J_2 + 2J_1, & \text{for } J_2/J_1 > 1/8. \end{cases} \quad (16)$$

The system is fully polarized when  $B > \tilde{J}$  (see Fig. 3(a) and (b)).

Switching on SOC but keeping  $\lambda$  lower than the critical value at the zero field such that the ground state has the spiral order, we find that the magnetization curve differs from the limit with  $\lambda \rightarrow 0$ . A small magnetic field brings down one of the  $J = 1$  triplet states and thus enhances the spiral magnetization component  $\mathbb{M}_\perp$  that would be suppressed by SOC, and at same time

brings a linear growth of the out-of-plane magnetization  $\mathbb{M}_z$ . As the field is further increased, the system enters a fully polarized state (see Fig. 3(c)), and  $\mathbb{M}_\perp$  is then suppressed. This explains the left part of the phase diagram in Fig. 3(a), where the coexisting region of  $\mathbb{M}_\perp$  and  $\mathbb{M}_z$  is dubbed ‘‘conical state’’.

When the strength of SOC is greater than the critical value, the mean-field ground state at the zero field is a spin-orbital singlet. The polarized moment  $\mathbb{M}_z$  still grows linearly as the magnetic field is switched on, while a nonzero  $\mathbb{M}_\perp$  only emerges at a critical field and shows a double-dome structure (see Fig. 3(d)). For an even stronger SOC, the  $M_\perp$  curve evolves into two separated domes, as shown in Fig. 3(e). This is what happens in the right part of the phase diagram in Fig. 3(a), where the system shows re-entrant transitions between the SOS and the conical state before being fully polarized when the field is very strong.

The peculiar double-dome structure of the magnetization and the re-entrant transitions under the magnetic field are intimately connected to the spin-orbit-entangled structure of the local moments. Let us consider the strong SOC limit where the single-ion ground state of the local moment is a spin-orbital singlet with a total moment  $J = 0$ . Due to different  $g$  factors for the orbital angular momentum and spin,  $H_{\text{Zeeman}}$  conserves  $J^z$  while mixing states with different  $J^z$ . This gives a direct consequence that the  $J^z = 0$  singlet state can gain energy from the growth of  $\mathbb{M}_z$  when the magnetic field is switched on [6]. As the magnetic field increases, it brings down a  $J^z = 1$  state from the triplets and a  $J^z = 2$  state from the higher quintuplets successively. Thus, the single-ion ground state level crossing happens twice, and the crossing points expand into to finite ranges due to the bandwidth brought by the exchange interaction, corresponding to the double-dome structure in the  $\mathbb{M}_\perp$  curve, which fuse together for large enough exchange interaction. This explains the structure of the magnetic phase diagram in Fig. 3(a).

It is illuminating to compare our results to that for the dimerized magnets. For  $S = 1/2$  dimerized magnets, the field could drive a Bose-Einstein condensation of triplons from the dimerized ground state [29], and the transition occurs at the point where the energy gap of the triplon is closed. Due to the local moment structure of the dimer with only singlet and triplets, there is only one dome in the  $\mathbb{M}_\perp$  curve, and the ground state level crossing only happens once. For  $S = 1$  dimerized magnets, the scenario is more similar to results here due to the existence of higher quintuplets, and one could expect the same double-dome structure in the  $\mathbb{M}_\perp$  curve. On the other hand, for both  $S = 1/2$  and  $S = 1$  dimerized magnets, since the magnetic field couples to the spins only, the Zeeman term conserves both  $S_{\text{tot}}^z$  and  $S_{\text{tot}}$  on each dimer. This implies that  $\mathbb{M}_z$  grows only within the domes in the  $\mathbb{M}_\perp$  curve, and becomes plateaus out of that [29–



tetrahedral environment	octahedral environment
$d^8 (e_g^4 t_{2g}^4)$ 	$d^4 (t_{2g}^4 e_g^0)$ 
$d^9 (e_g^4 t_{2g}^5)$ 	$d^5 (t_{2g}^5 e_g^0)$ 

TABLE I. The correspondence between different electron configurations in the tetrahedral and octahedral environments. The second row indicates the possibility of exploring physics similar to iridates and Kitaev physics [1, 34] in  $d^9$  materials [35].

32], which differs from results here.

The field response of our model is also quite different from that of  $\text{FeSc}_2\text{S}_4$ , where the magnetic order will be suppressed by applying the magnetic field, indicating a different entangled structure of the spin and the orbital degrees of freedom [3, 4]. All the three cases can be naturally understood from the evolution of the single-ion level scheme under the magnetic field that are summarized in the Supplementary material [27]. From our simple comparison, we immediately conclude that the double-dome structure in the  $M_{\perp}$  curve and the re-entrant transitions, together with the growth behavior of the magnetization  $M_z$ , reflect the unique entangled structure of the spin and the orbitals in  $H_{\text{soc}}$ .

*Uniaxial strain.*—We introduce the perturbation from the uniaxial strain that is modeled by  $H_{\text{Uni}} = -U \sum_i (L_i^z)^2$ . This term captures the low-temperature tetragonal distortion of  $\text{NiRh}_2\text{O}_4$  [16, 33] that modifies the tetrahedral crystal field of the  $\text{Ni}^{2+}$  ion in Fig. 1. This distortion, however, preserves the two-fold degeneracy of the  $xz$  and  $yz$  orbitals [23]. Within our mean-field theory, we find the critical strength of SOC is raised by  $U/3$  compared to the one without the uniaxial strain, *i.e.* the magnetic order is enhanced (see details in Supplementary materials [27]).

*Discussion.*—In summary, we propose a simple spin-orbital model for the diamond lattice antiferromagnet  $\text{NiRh}_2\text{O}_4$  and related systems, capturing the competition between the atomic SOC and the exchange interaction. We point out that this competition leads to a quantum criticality between the spin-orbital singlet and the magnetic ordered states. We further study the unique response behavior of our model to the magnetic field and the perturbation effect from the uniaxial strain.

The material  $\text{NiRh}_2\text{O}_4$  shows a Rln 6 magnetic entropy that is greater than the pure spin-1 moments [16], indicating the presence of additional (two-fold) orbital de-

grees of freedom. This was suggested to arise from the residual degeneracy of the  $xz$  and  $yz$  orbitals in the presence of the tetragonal distortion [23]. Since this is the orbital degeneracy in the  $t_{2g}$  manifold, the atomic SOC is active at the linear order. The tetragonal distortion was then included on top of the SOC and the exchange interactions. We expect our model to qualitatively describe the properties of the material and that the general physics revealed by this model is relevant to other similar materials. Due to the absence of obvious magnetic orders, the material is probably located on the spin-orbital singlet side. Various experimental probes can be useful to study the effect of spin-orbital entanglement and can probably drive the system to quantum criticality via pressures. The magnetic excitations in the SOS and the critical behaviors near the quantum criticality are detectable through the usual spectroscopic and thermodynamic measurements. The Higgs mode (or amplitude mode) is one of the characteristic properties associated with the criticality in our model, and can thus be probed by inelastic neutron scattering near the criticality but on the ordered side. This has actually been previously studied in dimerized magnet  $\text{TlCuCl}_3$  [36, 37] and the quasi-two-dimensional antiferromagnet  $\text{CaRu}_2\text{O}_4$  [38]. From the SOS side, one could use INS to detect the magnetic field dependence of the excitations, as it was performed for the powder sample of  $\text{FeSc}_2\text{S}_4$  [6]. A completely opposite tendency, however, is expected for  $\text{NiRh}_2\text{O}_4$ .

The atomic SOC acts quite similarly for the  $\text{Ni}^{2+}$  in the tetrahedral environment and the  $4d^4/5d^4$  electron configuration in the octahedral environment. From this observation, we list the correspondence between the electron configurations under these two crystal field environments in Table. I. This list can be further expanded with more examples. This correspondence immediately suggests some of the physics on one side may be extended to the other side. For instance, doping-induced ferromagnetism and unconventional superconductivity were proposed for the doped  $d^4$  systems such as  $\text{CaRu}_2\text{O}_4$  [18, 39]. Without much creativity, one may think such phenomena could be relevant for the doped  $d^8$  materials with the tetrahedral crystal field environments.

*Acknowledgments.*—We thank Juan Chamorro, Tyrel McQueen, Martin Mourigal and Oleg Tchernyshyov for discussion. This work is supported by the Ministry of Science and Technology of China with the Grant No.2016YFA0301001, the Start-Up Fund and the First-Class University Construction Fund of Fudan University, and the Thousand-Youth-Talent Program of China.

\* [gangchen.physics@gmail.com](mailto:gangchen.physics@gmail.com)

[1] William Witczak-Krempa, Gang Chen, Yong Baek Kim, and Leon Balents, “Correlated Quantum Phenomena in

- the Strong Spin-Orbit Regime,” *Annual Review of Condensed Matter Physics* **5**, 57–82 (2014).
- [2] Giniyat Khaliullin, Sadamichi Maekawa, Stewart Edward Barnes, Sumio Ishihara, Takami Tohyama, and Wataru Koshibae, *Physics of Transition Metal Oxides* (Springer, 2004).
- [3] Gang Chen, Andreas P. Schnyder, and Leon Balents, “Excitation spectrum and magnetic field effects in a quantum critical spin-orbital system: The case of  $\text{FeSc}_2\text{S}_4$ ,” *Phys. Rev. B* **80**, 224409 (2009).
- [4] Gang Chen, Leon Balents, and Andreas P. Schnyder, “Spin-Orbital Singlet and Quantum Critical Point on the Diamond Lattice:  $\text{FeSc}_2\text{S}_4$ ,” *Phys. Rev. Lett.* **102**, 096406 (2009).
- [5] V. Fritsch, J. Hemberger, N. Büttgen, E.-W. Scheidt, H.-A. Krug von Nidda, A. Loidl, and V. Tsurkan, “Spin and Orbital Frustration in  $\text{MnSc}_2\text{S}_4$  and  $\text{FeSc}_2\text{S}_4$ ,” *Phys. Rev. Lett.* **92**, 116401 (2004).
- [6] A. Biffin, Ch. Rüegg, J. Embs, T. Guidi, D. Cheptiakov, A. Loidl, V. Tsurkan, and R. Coldea, “Magnetic Field Dependence of Excitations Near Spin-Orbital Quantum Criticality,” *Phys. Rev. Lett.* **118**, 067205 (2017).
- [7] K. W. Plumb, J. R. Morey, J. A. Rodriguez-Rivera, Hui Wu, A. A. Podlesnyak, T. M. McQueen, and C. L. Broholm, “Antiferromagnetic and Orbital Ordering on a Diamond Lattice Near Quantum Criticality,” *Phys. Rev. X* **6**, 041055 (2016).
- [8] Chandan Setty, Zhidong Leong, Shuyi Zhang, and Philip W. Phillips, “Absence of nematic ordering transition in a diamond lattice: Application to  $\text{FeSc}_2\text{S}_4$ ,” *Phys. Rev. B* **95**, 020403 (2017).
- [9] A. Krimmel, M. Mücksch, V. Tsurkan, M. M. Koza, H. Mutka, and A. Loidl, “Vibronic and Magnetic Excitations in the Spin-Orbital Liquid State of  $\text{FeSc}_2\text{S}_4$ ,” *Phys. Rev. Lett.* **94**, 237402 (2005).
- [10] L. Mittelstädt, M. Schmidt, Zhe Wang, F. Mayr, V. Tsurkan, P. Lunkenheimer, D. Ish, L. Balents, J. Deisenhofer, and A. Loidl, “Spin-orbital and quantum criticality in  $\text{FeSc}_2\text{S}_4$ ,” *Phys. Rev. B* **91**, 125112 (2015).
- [11] S. Sarkar, T. Maitra, Roser Valentí, and T. Saha-Dasgupta, “Comparative study of  $\text{FeCr}_2\text{S}_4$  and  $\text{FeSc}_2\text{S}_4$ : Spinels with orbitally active  $A$  site,” *Phys. Rev. B* **82**, 041105 (2010).
- [12] N. J. Laurita, J. Deisenhofer, LiDong Pan, C. M. Morris, M. Schmidt, M. Johnsson, V. Tsurkan, A. Loidl, and N. P. Armitage, “Singlet-Triplet Excitations and Long-Range Entanglement in the Spin-Orbital Liquid Candidate  $\text{FeSc}_2\text{S}_4$ ,” *Phys. Rev. Lett.* **114**, 207201 (2015).
- [13] George Jackeli and Giniyat Khaliullin, “Magnetically Hidden Order of Kramers Doublets in  $d^1$  Systems:  $\text{Sr}_2\text{VO}_4$ ,” *Phys. Rev. Lett.* **103**, 067205 (2009).
- [14] Keisuke Matsuura, Hajime Sagayama, Amane Uehara, Yoichi Nii, Ryoichi Kajimoto, Kazuya Kamazawa, Kazuhiko Ikeuchi, Sungdae Ji, Nobuyuki Abe, and Taka-hisa Arima, “Spin-Orbital Correlated Dynamics in the Spinel-Type Vanadium Oxide  $\text{MnV}_2\text{O}_4$ ,” *Phys. Rev. Lett.* **119**, 017201 (2017).
- [15] L. D. Tung, A. Ivanov, J. Schefer, M. R. Lees, G. Balakrishnan, and D. McK. Paul, “Spin, orbital ordering, and magnetic dynamics of  $\text{LaVO}_3$ : Magnetization, heat capacity, and neutron scattering studies,” *Phys. Rev. B* **78**, 054416 (2008).
- [16] J. R. Chamorro, L. Ge, J. Flynn, M. A. Subramanian, M. Mourigal, and T. M. McQueen, “Frustrated spin one on a diamond lattice in  $\text{NiRh}_2\text{O}_4$ ,” *Phys. Rev. Materials* **2**, 034404 (2018).
- [17] Gang Chen and Leon Balents, “Spin-orbit coupling in  $d^2$  ordered double perovskites,” *Phys. Rev. B* **84**, 094420 (2011).
- [18] Giniyat Khaliullin, “Excitonic Magnetism in Van Vleck-type  $d^4$  Mott Insulators,” *Phys. Rev. Lett.* **111**, 197201 (2013).
- [19] Kliment I Kugel’ and D I Khomski, “The Jahn-Teller effect and magnetism: transition metal compounds,” *Soviet Physics Uspekhi* **25**, 231 (1982).
- [20] Doron Bergman, Jason Alicea, Emanuel Gull, Simon Trebst, and Leon Balents, “Order-by-disorder and spiral spin-liquid in frustrated diamond-lattice antiferromagnets,” *Nature Physics* **3**, 487 (2007).
- [21] SungBin Lee and Leon Balents, “Theory of the ordered phase in  $A$ -site antiferromagnetic spinels,” *Phys. Rev. B* **78**, 144417 (2008).
- [22] Lucile Savary, Emanuel Gull, Simon Trebst, Jason Alicea, Doron Bergman, and Leon Balents, “Impurity effects in highly frustrated diamond-lattice antiferromagnets,” *Phys. Rev. B* **84**, 064438 (2011).
- [23] Gang Chen, “Quantum paramagnet and frustrated quantum criticality in a spin-one diamond lattice antiferromagnet,” *Phys. Rev. B* **96**, 020412 (2017).
- [24] Finn Lasse Buessen, Max Hering, Johannes Reuther, and Simon Trebst, “Quantum Spin Liquids in Frustrated Spin-1 Diamond Antiferromagnets,” *Phys. Rev. Lett.* **120**, 057201 (2018).
- [25] Jean-Sébastien Bernier, Michael J. Lawler, and Yong Baek Kim, “Quantum Order by Disorder in Frustrated Diamond Lattice Antiferromagnets,” *Phys. Rev. Lett.* **101**, 047201 (2008).
- [26] Masashige Matsumoto, B. Normand, T. M. Rice, and Manfred Sigrist, “Field- and pressure-induced magnetic quantum phase transitions in  $\text{TlCuCl}_3$ ,” *Phys. Rev. B* **69**, 054423 (2004).
- [27] See Supplemental Material for a detailed discussion.
- [28] G. Chen, M. Hermele, and L. Radzihovsky, “Frustrated Quantum Critical Theory of Putative Spin-Liquid Phenomenology in  $6H-B-Ba_3\text{NiSb}_2\text{O}_9$ ,” *Phys. Rev. Lett.* **109**, 016402 (2012).
- [29] Vivien Zapf, Marcelo Jaime, and C. D. Batista, “Bose-Einstein condensation in quantum magnets,” *Rev. Mod. Phys.* **86**, 563–614 (2014).
- [30] E. C. Samulon, Y. Kohama, R. D. McDonald, M. C. Shapiro, K. A. Al-Hassanieh, C. D. Batista, M. Jaime, and I. R. Fisher, “Asymmetric Quintuplet Condensation in the Frustrated  $S = 1$  Spin Dimer Compound  $\text{Ba}_3\text{Mn}_2\text{O}_8$ ,” *Phys. Rev. Lett.* **103**, 047202 (2009).
- [31] M. Uchida, H. Tanaka, H. Mitamura, F. Ishikawa, and T. Goto, “High-field magnetization process in the  $S = 1$  quantum spin system  $\text{Ba}_3\text{Mn}_2\text{O}_8$ ,” *Phys. Rev. B* **66**, 054429 (2002).
- [32] Masahiro Uchida, Hidekazu Tanaka, Mikhail I. Bartashevich, and Tsuneaki Goto, “Singlet Ground State and Magnetization Plateaus in  $\text{Ba}_3\text{Mn}_2\text{O}_8$ ,” *Journal of the Physical Society of Japan* **70**, 1790–1793 (2001).
- [33] Sumiko Horiuti and Syhei Miyahara, “Tetragonal Distortion of  $\text{NiRh}_2\text{O}_4$ ,” *Journal of the Physical Society of Japan* **19**, 423–424 (1964).
- [34] Simon Trebst, “Kitaev materials,” arXiv:1701.07056 (2017).
- [35] L. Ge, J. Flynn, J. A. M. Paddison, M. B. Stone,

- S. Calder, M. A. Subramanian, A. P. Ramirez, and M. Mourigal, “Spin order and dynamics in the diamond-lattice Heisenberg antiferromagnets  $\text{CuRh}_2\text{O}_4$  and  $\text{CoRh}_2\text{O}_4$ ,” *Phys. Rev. B* **96**, 064413 (2017).
- [36] P. Merchant, B. Normand, K. W. Krämer, M. Boehm, D. F. McMorrow, and Ch. Rüegg, “Quantum and classical criticality in a dimerized quantum antiferromagnet,” *Nature Physics* **10**, 373 (2014).
- [37] Ch. Rüegg, B. Normand, M. Matsumoto, A. Furrer, D. F. McMorrow, K. W. Krämer, H. U. Güdel, S. N. Gvasaliya, H. Mutka, and M. Boehm, “Quantum Mag-

- nets under Pressure: Controlling Elementary Excitations in  $\text{TlCuCl}_3$ ,” *Phys. Rev. Lett.* **100**, 205701 (2008).
- [38] A. Jain, M. Krautloher, J. Porras, G. H. Ryu, D. P. Chen, D. L. Abernathy, J. T. Park, A. Ivanov, J. Chaloupka, G. Khaliullin, B. Keimer, and B. J. Kim, “Higgs mode and its decay in a two-dimensional antiferromagnet,” *Nature Physics* **13**, 633 (2017).
- [39] Jiří Chaloupka and Giniyat Khaliullin, “Doping-Induced Ferromagnetism and Possible Triplet Pairing in  $d^4$  Mott Insulators,” *Phys. Rev. Lett.* **116**, 017203 (2016).

Supplementary materials for “Emergent quantum criticality from spin-orbital entanglement in  $d^8$  Mott insulators: the case of a diamond lattice antiferromagnet”

- I. Details on flavor-wave approach  
 II. Effect of uniaxial strain  
 III. Response behavior to magnetic field

## I. DETAILS ON FLAVOR-WAVE APPROACH

In this section we describe the flavor-wave approach to the diamond lattice system

$$H = \sum_{\langle ij \rangle} J_1 \mathbf{S}_i \cdot \mathbf{S}_j + \sum_{\langle\langle ij \rangle\rangle} J_2 \mathbf{S}_i \cdot \mathbf{S}_j + \lambda \sum_i \mathbf{L}_i \cdot \mathbf{S}_i, \quad (17)$$

with  $S = 1$  and  $L = 1$ . In this approach, one starts from the spin-orbital singlet side, i.e. the large  $\lambda$  limit, and studies its excitations and instability. Consider the low-energy space on each site consisting of the  $J = 0$  singlet and the  $J = 1$  triplets, and project out the  $J = 2$  quintuplets, we introduce four flavors of bosons  $s_i, t_{ix}, t_{iy}, t_{iz}$  on each site  $i$  that are defined as

$$s_i^\dagger |0\rangle \equiv |0, 0\rangle_i, \quad (18)$$

$$t_{ix}^\dagger |0\rangle \equiv \frac{i}{\sqrt{2}} (|1, 1\rangle_i - |1, -1\rangle_i), \quad (19)$$

$$t_{iy}^\dagger |0\rangle \equiv \frac{1}{\sqrt{2}} (|1, 1\rangle_i + |1, -1\rangle_i), \quad (20)$$

$$t_{iz}^\dagger |0\rangle \equiv -i |1, 0\rangle_i, \quad (21)$$

where the states are labeled  $|J, J^z\rangle$  and  $|0\rangle$  is the vacuum state. A local Hilbert space constraint  $s_i^\dagger s_i + \sum_\alpha t_{i\alpha}^\dagger t_{i\alpha} = 1$  is imposed with  $\alpha = x, y, z$ . The original spin and orbital operators are then represented

as

$$S_i^x = \Psi_i^\dagger \begin{pmatrix} 0 & -i\sqrt{\frac{2}{3}} & 0 & 0 \\ i\sqrt{\frac{2}{3}} & 0 & 0 & 0 \\ 0 & 0 & 0 & -\frac{i}{2} \\ 0 & 0 & \frac{i}{2} & 0 \end{pmatrix} \Psi_i, \quad (22)$$

$$S_i^y = \Psi_i^\dagger \begin{pmatrix} 0 & 0 & -i\sqrt{\frac{2}{3}} & 0 \\ 0 & 0 & 0 & \frac{i}{2} \\ i\sqrt{\frac{2}{3}} & 0 & 0 & 0 \\ 0 & -\frac{i}{2} & 0 & 0 \end{pmatrix} \Psi_i, \quad (23)$$

$$S_i^z = \Psi_i^\dagger \begin{pmatrix} 0 & 0 & 0 & -i\sqrt{\frac{2}{3}} \\ 0 & 0 & -\frac{i}{2} & 0 \\ 0 & \frac{i}{2} & 0 & 0 \\ i\sqrt{\frac{2}{3}} & 0 & 0 & 0 \end{pmatrix} \Psi_i, \quad (24)$$

and

$$\mathbf{L}_i \cdot \mathbf{S}_i = \Psi_i^\dagger \begin{pmatrix} -2 & 0 & 0 & 0 \\ 0 & -1 & 0 & 0 \\ 0 & 0 & -1 & 0 \\ 0 & 0 & 0 & -1 \end{pmatrix} \Psi_i, \quad (25)$$

$$(L_i^z)^2 = \Psi_i^\dagger \begin{pmatrix} \frac{2}{3} & 0 & 0 & 0 \\ 0 & \frac{1}{2} & 0 & 0 \\ 0 & 0 & \frac{1}{2} & 0 \\ 0 & 0 & 0 & 1 \end{pmatrix} \Psi_i, \quad (26)$$

with  $\Psi_i = (s_i, t_{ix}, t_{iy}, t_{iz})^T$ .

In the spin-orbital singlet phase, the singlet boson  $s_i$  is condensed with  $\langle s_i \rangle \equiv s \neq 0$  and one can further require

$$s \rightarrow \left[ 1 - \frac{1}{N} \sum_{i\alpha} t_{i\alpha}^\dagger t_{i\alpha} \right]^{\frac{1}{2}} \approx 1 - \frac{1}{2N} \sum_{i\alpha} t_{i\alpha}^\dagger t_{i\alpha}, \quad (27)$$

which takes the local Hilbert space constraint into account. Here  $N$  is the number of sites.

With the above reformulation of the spin variables, we keep terms up to the second order and obtain a flavor-

wave mean-field Hamiltonian for the triplet excitations,

$$\begin{aligned}
H_{\text{FMF}} = & \sum_{\langle ij \rangle, \alpha} \frac{2J_1}{3} \left( t_{i\alpha}^\dagger t_{j\alpha} + t_{i\alpha}^\dagger t_{j\alpha}^\dagger + \text{h.c.} \right) \\
& + \sum_{\langle\langle ij \rangle\rangle, \alpha} \frac{2J_2}{3} \left( t_{i\alpha}^\dagger t_{j\alpha} + t_{i\alpha}^\dagger t_{j\alpha}^\dagger + \text{h.c.} \right) \\
& + \lambda \sum_{i\alpha} t_{i\alpha}^\dagger t_{i\alpha}. \tag{28}
\end{aligned}$$

The triplon excitation can be readily found as

$$\omega^\pm(\mathbf{q}) = \lambda^{\frac{1}{2}} (\lambda + 4J_{\mathbf{q}}^\pm/3)^{\frac{1}{2}}, \tag{29}$$

with  $J_{\mathbf{q}}^\pm \equiv J_2 \sum_{\mathbf{b}_i} e^{i\mathbf{q}\cdot\mathbf{b}_i} \pm J_1 |\sum_{\mathbf{a}_i} e^{i\mathbf{q}\cdot\mathbf{a}_i}|$ , and  $\{\mathbf{a}_i\}$  ( $\{\mathbf{b}_i\}$ ) refer to the first (second) neighbor vectors. Both  $\omega^\pm(\mathbf{q})$  are three-fold degenerate and the minimum of  $\omega^-(\mathbf{q})$  is determined by minimizing  $J_{\mathbf{q}}^-$ . For  $J_2/J_1 < 1/8$ , a single minimum is realized at the  $\Gamma$  point, and for  $J_2/J_1 > 1/8$ , the minima are extensively degenerate and realized on the ‘‘spiral surface’’.

For the diamond lattice, the first neighbor vectors  $\{\mathbf{a}_i\}$  are  $\{\frac{1}{4}[111], \frac{1}{4}[\bar{1}\bar{1}\bar{1}], \frac{1}{4}[\bar{1}1\bar{1}], \frac{1}{4}[\bar{1}\bar{1}1]\}$  and three FCC lattice vectors are  $\frac{1}{2}[011], \frac{1}{2}[101]$  and  $\frac{1}{2}[110]$ , then

$$J_{\mathbf{q}}^\pm = 4J_2\Lambda(\mathbf{q}) \pm 2J_1\sqrt{\Lambda(\mathbf{q}) + 1}, \tag{30}$$

with

$$\begin{aligned}
\Lambda(\mathbf{q}) = & \cos\left(\frac{q_x}{2}\right) \cos\left(\frac{q_y}{2}\right) + \cos\left(\frac{q_x}{2}\right) \cos\left(\frac{q_z}{2}\right) \\
& + \cos\left(\frac{q_y}{2}\right) \cos\left(\frac{q_z}{2}\right). \tag{31}
\end{aligned}$$

The spiral surface is given by

$$\Lambda(\mathbf{q}) = \frac{J_1^2}{16J_2^2} - 1. \tag{32}$$

## II. EFFECT OF UNIAXIAL STRAIN

With the uniaxial strain term

$$H_{\text{Uni}} = - \sum_i U(L_i^z)^2, \tag{33}$$

the flavor-wave mean-field Hamiltonian becomes

$$H'_{\text{FMF}} = H_{\text{FMF}} + \sum_{i\alpha} \frac{U}{6} t_{i\alpha}^\dagger t_{i\alpha} - \sum_i \frac{U}{2} t_{iz}^\dagger t_{iz}. \tag{34}$$

The uniaxial strain lowers the energy of the  $t_{i,z}$  mode and splits the three-fold degeneracy. The dispersion of the triplon excitation now reads

$$\omega_z^\pm(\mathbf{q}) = (\lambda - U/3)^{\frac{1}{2}} (\lambda - U/3 + 4J_{\mathbf{q}}^\pm/3)^{\frac{1}{2}}, \tag{35}$$

$$\omega_{xy}^\pm(\mathbf{q}) = (\lambda + U/6)^{\frac{1}{2}} (\lambda + U/6 + 4J_{\mathbf{q}}^\pm/3)^{\frac{1}{2}}, \tag{36}$$

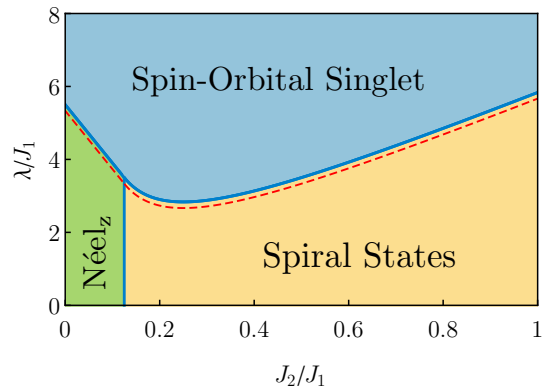


FIG. 4. (Color online.) The phase diagram with uniaxial strain  $U/J_1 = 0.5$ . The Néel<sub>z</sub> phase indicates that the Néel order is along the  $z$  axis. For comparison, the red (dashed) line gives the original boundary between the SOS and the magnetic ordered phases when  $U/J_1 = 0$ .

where  $\omega_z^\pm(\mathbf{q})$  are not degenerate and  $\omega_{xy}^\pm(\mathbf{q})$  are two-fold degenerate.

The triplon gap is closed at a critical SOC and the effect of  $U$  term is to raise the critical strength of SOC by  $U/3$ , i.e. to enhance the magnetic order, see Fig. 4. For  $J_2/J_1 < 1/8$ , Néel order along the  $z$  axis is stabilized from condensing  $\omega_z^-(\mathbf{q})$  at  $\Gamma$  point. For  $J_2/J_1 > 1/8$ , the minima are realized on the ‘‘spiral surface’’ and generally the critical modes prefer a magnetic order with nonuniform magnitude on each site. We dub this ordered region ‘‘spiral state’’ in Fig. 4.

## III. RESPONSE BEHAVIOR TO MAGNETIC FIELD

In this section, we discuss the response behavior to magnetic field of (1) our simplified model for  $\text{NiRh}_2\text{O}_4$ , (2) the spin  $S = 2$  diamond lattice antiferromagnet  $\text{FeSc}_2\text{S}_4$ , (3) spin-1/2 and spin-1 dimerized magnets.

For each system, the Hamiltonian can be separated into the single-ion part  $H_0$  and the exchange part  $H_{\text{ex}}$  (for dimerized magnets [36], the building block is the spin dimer with two spin-1/2 moments,  $H_0$  is the isolated dimer part and  $H_{\text{ex}}$  should be understood as inter-dimer exchange interactions). Whether the initial state of the system at the zero field is a non-magnetic state or a magnetic ordered state depends on the strength of  $H_{\text{ex}}$ . When  $H_{\text{ex}}$  is small, in all three cases the system starts from the non-magnetic singlet side and finally becomes fully polarized. The response behavior is directly related to the single-ion energy level scheme evolution under the magnetic field, as we show in Fig. 5.

As in main text, we assume that the magnetic field is applied along the  $\hat{z}$  direction, and  $\langle \mathbf{S}_i \rangle = \mathbb{M}_\perp \hat{n}_i + \mathbb{M}_z \hat{z}$ , where  $\hat{n}_i$  is a unit vector on the  $xy$  plane. So  $\mathbb{M}_\perp$  and  $\mathbb{M}_z$  represent the magnetizations on the  $xy$  plane and along



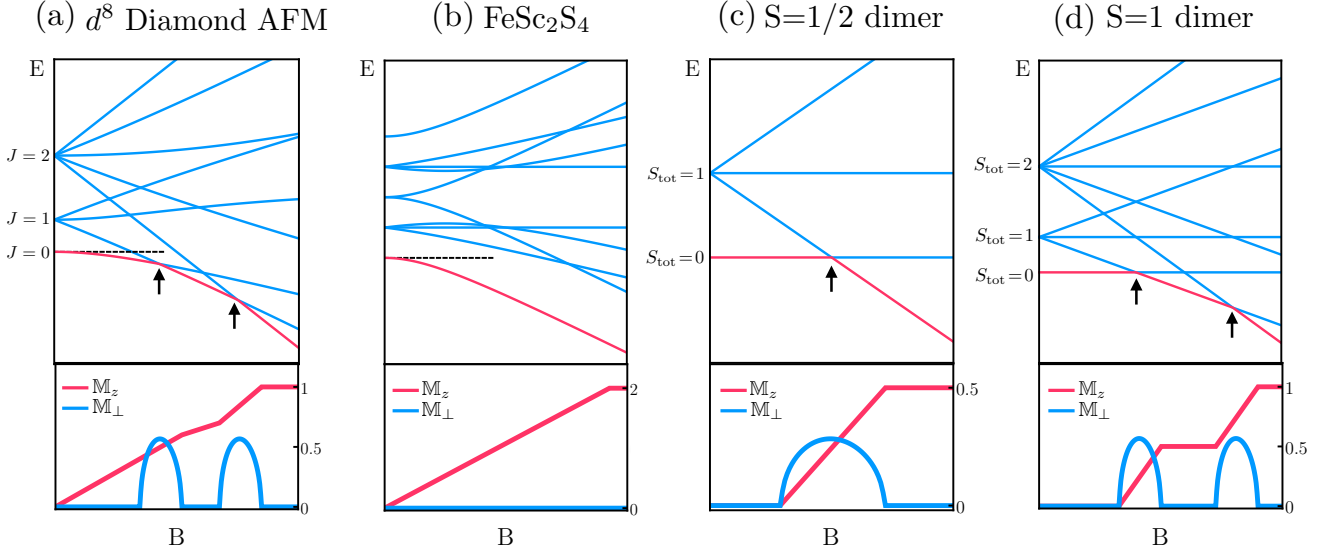


FIG. 5. (Color online.) Single-ion energy level schemes (upper panels) and schematic magnetization curves (lower panels) for (a)  $d^8$  diamond AFM, (b) The  $S = 1$  diamond lattice antiferromagnet  $\text{FeSc}_2\text{S}_4$ , (c) spin-1/2 dimerized magnets, (d) spin-1 dimerized magnets [30]. See discussion in text.

the  $z$  axis, respectively.

The single-ion Hamiltonian of our simplified model for  $\text{NiRh}_2\text{O}_4$  reads

$$\begin{aligned} H_0 &= \lambda \sum_i \mathbf{L}_i \cdot \mathbf{S}_i - \sum_i B(L_i^z + 2S_i^z) \\ &= \lambda \sum_i (\mathbf{J}_i)^2 / 2 - \sum_i B(J_i^z + S_i^z), \end{aligned} \quad (37)$$

with  $\lambda > 0$ , spin  $S = 1$ , the effective orbital angular momentum  $L = 1$  and  $\mathbf{J}_i \equiv \mathbf{L}_i + \mathbf{S}_i$ . At the zero field, the SOC term splits the single-ion energy levels to the lowest  $J = 0$  singlet, higher  $J = 1$  triplets and  $J = 2$  quintuplets. Since  $J^z$  is conserved and  $J$  is not, the singlet evolves to a  $\langle J \rangle \neq 0$  state and gains energy from the growth of  $M_z$ , when the magnetic field is switched on. As the magnetic field increasing, it brings down a  $J^z = 1$  state from the triplets and a  $J^z = 2$  state from the quintuplets successively, and the ground state level crossing happens twice. For small but nonzero  $H_{\text{ex}}$ , the crossing points expand to finite ranges due to the bandwidth brought by the exchange interaction, leading to the double-dome structure in the  $M_{\perp}$  curve, see Fig. 5(a), (e). For stronger  $H_{\text{ex}}$ , two domes will fuse together.

The single-ion Hamiltonian of  $\text{FeSc}_2\text{S}_4$  can be modeled as [3]

$$\begin{aligned} H_0 &= -\frac{\lambda}{3} \sum_i \left\{ \sqrt{3}T_i^x [(S_i^x)^2 - (S_i^y)^2] + T_i^z [3(S_i^z)^2 - S_i^2] \right\} \\ &\quad - \sum_i BS_i^z, \end{aligned} \quad (38)$$

with  $\lambda > 0$ , spin  $S = 2$  and the pseudospin  $T = 1/2$ ,

where  $T$  acts on the  $x^2 - y^2$  and  $3z^2 - r^2$  orbitals in the  $e_g$  subspace. The orbital angular momentum is quenched and the magnetic field couples to spin only. Again the lowest singlet state at zero-field can gain energy from the polarization when the magnetic field is switched on. Moreover, it adiabatically evolves to the fully polarized state without level crossing, so  $M_{\perp}$  remains zero, see Fig. 5(b), (f). For strong enough  $H_{\text{ex}}$ , the initial state of the system is a magnetic ordered state with nonzero  $M_{\perp}$ . The magnetic field is to suppress the magnetic order [3], leading to a monotonic decrease of  $M_{\perp}$ .

For dimerized magnets, one has

$$\begin{aligned} H_0 &= J_0 \sum_i \mathbf{S}_{i,1} \cdot \mathbf{S}_{i,2} - \sum_i B(S_{i,1}^z + S_{i,2}^z) \\ &= J_0 \sum_i (\mathbf{S}_{i,\text{tot}})^2 / 2 - \sum_i BS_{i,\text{tot}}^z, \end{aligned} \quad (39)$$

with  $J_0 > 0$ . Here,  $\mathbf{S}_{i,1}$  and  $\mathbf{S}_{i,2}$  are two spins on the dimer  $i$ . At zero field,  $J_0$  splits the single-ion energy levels to the lowest  $S_{\text{tot}} = 0$  singlet and higher high-spin multiplets. Due to Zeeman splitting, the magnetic field brings down high- $S_{\text{tot}}^z$  states and the ground state level crossing happens. The same argument as that for  $\text{NiRh}_2\text{O}_4$  can explain the single- (double-) dome structure in the  $M_{\perp}$  curve of spin-1/2 (spin-1) dimerized magnets. Interestingly, since both  $S_{\text{tot}}$  and  $S_{\text{tot}}^z$  are conserved,  $M_z$  can only grow within the ranges corresponding to level crossings, i.e. within the domes in the  $M_{\perp}$  curve, and becomes plateaus out of that [26, 30]. Please refer Fig. 5(c), (g) ((d), (h)) for the spin-1/2 (spin-1) case.